Advanced Robotics

ISSN: 0169-1864 (Print) 1568-5535 (Online) Journal homepage: http://www.tandfonline.com/loi/tadr20

Combined Inverse Kinematic and Static Analysis and Optimal Design of a Cable-Driven Mechanism with a Spring Spine

Bingtuan Gao , Jing Xu , Jianguo Zhao & Ning Xi

To cite this article: Bingtuan Gao , Jing Xu , Jianguo Zhao & Ning Xi (2012) Combined Inverse Kinematic and Static Analysis and Optimal Design of a Cable-Driven Mechanism with a Spring Spine, Advanced Robotics, 26:8-9, 923-946

To link to this article: http://dx.doi.org/10.1163/156855312X633048

Published online: 24 Jul 2012.

VSP

Advanced Robotics 26 (2012) 923–946

ADVANCED ROBOTICS
brill.nl/ar

Full paper

Combined Inverse Kinematic and Static Analysis and Optimal Design of a Cable-Driven Mechanism with a Spring Spine

Bingtuan Gao [a,b,*], **Jing Xu** [b,c], **Jianguo Zhao** [b] **and Ning Xi** [b]

[a] School of Electrical and Engineering, Southeast University, Nanjing 210096, P. R. China

[b] Department of Electrical and Computer Engineering, Michigan State University, East Lansing, MI 48824, USA

[c] Department of Precision Instruments and Mechanology, Tsinghua University, Beijing 100084, P. R. China

Received 28 April 2011; accepted 29 June 2011

Abstract

A special humanoid neck with low motion noise requirements yields a cable-driven parallel mechanism to imitate the rotational motion of a human neck. The fixed base and moving platform of the mechanism are connected by four cables and a column compression spring. The four cables are actuated separately, while the spring can support weight on the moving platform. Although similar mechanisms exist in the literature, the analysis of them is scarce because a flexible spring instead of a rigid kinematic chain is used as the spine. With the spring's lateral buckling motion, a new approach must be adopted to solve the kinematics. In this paper, we propose a method that combines the kinematics with the statics to solve them simultaneously. The configuration of the moving platform is parameterized with four parameters, one of which is considered as parasitic motion. Using the spring's lateral buckling equation, we can obtain the parasitic motion and solve the inverse position problem. The optimal design for cable placements is then performed to minimize the actuation force. The method in this paper provides a novel way to analyze parallel mechanisms with a spring spine and it can be applied to other mechanisms with flexible spines.

Keywords

Cable-driven, parallel mechanism, kinematics, spring lateral buckling, optimal design

1. Introduction

The mechanism analyzed in this paper comes from a biomimetic humanoid neck system with low motion noise requirements to investigate the acoustic issues dur-

* To whom correspondence should be addressed. E-mail: gaobingtuan@seu.edu.cn

 DOI:10.1163/156855312X633048

ing motion. In battlefields or other harmful environments, people always need to wear respirators and chemical-resistant jackets to survive under hostile conditions. In this case, when moving their heads, they inevitably suffer from noise produced by such respirators and jackets. These noises may obscure people's hearing of useful information and make them perform wrong actions, resulting in catastrophic consequences. Therefore, it is critical to analyze the effect of such noise on a human's hearing. To conduct such an acoustic investigation, a person, tediously enough, should wear respirators and jackets to perform repetitive head movements. Moreover, the labor cost is quite expensive if the experiments are performed many times. A better method is to use a robot head for such experiments. To make the experiments with a robot head identical to those with humans, the robot head should have the same functions as a human head, which includes the following two key requirements:

(i) The robot head should have the same movement degree of freedom (d.o.f.) and motion range as a human.

(ii) The robot head should, like the human head, not make noises itself during the movements without wearing equipment such as respirators or jackets.

The second requirement is critical because, in order to examine the noise effect of wearing equipment, all the other noises should be eliminated as much as possible. An illustration of the robot head for such an acoustic experiment is shown in Fig. 1, where a sound level meter is used to measure the noise. Other advanced equipment such as a sound recording system can be employed to record the noise [1].

The first requirement involves the principles for human head movements, which have been studied extensively in the biomechanics field. Clinical studies show that the movements result from the cervical spine consisting of seven vertebrae. This structure, which can be considered as a multi-joint serial mechanism, has 3 rotational d.o.f. plus coupled translational motion in each axis due to the flexible structure of the cervical spine [2]. It is rather expensive and difficult to obtain exactly the same motion of a human head. In practice, people usually consider the head just to have 3 (roll, pitch and yaw) rotational d.o.f.

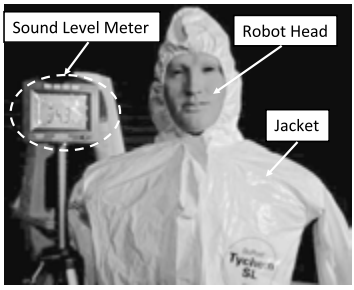

Figure 1. Illustration of using the low motion noise robot head to investigate acoustic issues.

A number of robot heads satisfying the movement requirements have been built in the context of humanoid robots in the past decade. They can all be classified into two categories: serial and parallel. For a serial head, each d.o.f. of the head is controlled independently. In the design of ARMAIII, the head is a 4-rotational-d.o.f. serial mechanism with 3 d.o.f. at the base and 1 d.o.f. at the top [3]. The Albert HUBO [4], the Dav [5], and the final version of iCub [6] all have 3-d.o.f. serial necks. The parallel head is based on a parallel mechanism, which consists of a moving platform connected to a fixed base by several identical actuated kinematic chains. The head is attached to the moving platform which has d.o.f. with respect to the fixed base. The head mechanism of SAYA is made up of a coil spring to support the head and several pneumatic artificial muscles placed around the spring to actuate the head [7]. For the iCub robot, aside from the serial neck mentioned above, two parallel mechanisms are implemented for the neck. The first one is based on a compression spring with three actuated cables separated 120° apart; the second one uses a 3-d.o.f. parallel mechanism with a central passive spherical strut [6]. The James humanoid robot also has a head similar to the first parallel mechanism of iCub [8].

Although all the heads in the above papers can realize the head motion, they fail to consider the second acoustic requirement. An exception is the acoustical telepresence robot presented in Ref. [9]. This robot is used to reconstruct the sound environment for a listener at a remote location and follow the listener's head motion at the same time. The robot is driven by motors *via* cable and pulley systems. Since no gears are used in the robot, the noise from the robot motion can be low. Nevertheless, the motors, installed right under the head, can still generate considerable noise. The feasibility of using the ultrasonic servomotor to replace the traditional motor is also investigated by the same group [10].

Based on the two requirements and the shortcomings for existing humanoid heads, we propose a mechanism shown in Fig. 2, which consists of a fixed plate and a mobile plate connected by four cables and a column compression spring. The fixed plate is connected to a torso, which is not shown in Fig. 2, while the mobile

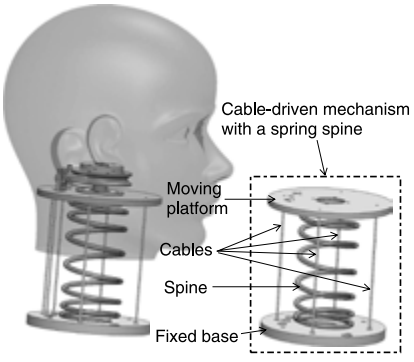

Figure 2. Overview of the robotic neck mechanism design.

plate is connected to the head. The mobile plate in Fig. 2 has 2 rotational d.o.f., which can make the head rotate in a specified direction with a desired amplitude. In order to have a rotational d.o.f. perpendicular to the mobile plate plane, another revolute joint with its axis perpendicular to the mobile plate is used. This revolute joint is driven by another two cables for bidirectional rotation. All the cables are actuated by motors in a sound insulation box far away from the head. As a result, no mechanical part exists near the head and the motion noise will be quite low at the head. Note that the whole mechanism is shown on the left side of Fig. 2, while the mechanism without the revolute joint is shown on the right side. Since this paper will focus on the analysis for the mechanism without the revolute joint, unless otherwise stated, reference to Fig. 2 will indicate the mechanism on the right.

The use of a spring as the spine in the cable-driven mechanism comes from the two requirements for robot head. For the first requirement, the spring can make the robot head move in a similar way to a human head. With a cervical spine made up of seven vertebrae, the rotating center for a human head is not fixed. Therefore, the method of using a spherical joint to connect the fixed and mobile plate cannot be adopted, which will have a fixed rotation center. Although a series of spherical joints can be used, it is quite complicated [11]. The spring provides a simple solution because it can be considered as the cervical spine of a human neck with the active turns as the seven vertebrae. For the second requirement, the spring will not generate any noise during the motion once it is rigidly attached to the fixed and mobile plate. This cannot be realized by mechanical joints because they may produce some noise if the payload is quite large.

The mechanism shown in Fig. 2 is a cable-driven mechanism. This type of mechanism has recently attracted a lot of research interest. Compared to traditional mechanisms, cable-driven mechanisms are relatively simple in form and possess some valuable characteristics, such as large workspace, low inertia, high payload-to-weight ratio, transportability, reconfigurability and fully remote actuation [12]. Consequently, cable-driven mechanisms are well-suited for many applications, such as surveillance of large-scale places, interaction with disaster sites and manipulation of heavy payloads. Research has been performed based on practical implementation and a large number of cable-driven mechanisms have been developed, such as the RoboCrane for moving heavy loads over a large workspace [13], the WARP manipulator for high-speed assembly of lightweight objects [14], the large-scale FAST system for a large radio telescope receiver [15], the NIMS3D cabled robot for actuated sensing applications [16] and the flexible link mechanism for keeping stiffness against load [17]. There are lots of prior studies on kinematics and workspace [18, 19], force-closure analysis [20, 21], optimal cable tension distribution [22, 23], and dynamics and control [15, 24].

The cable-driven mechanism shown in Fig. 2 belongs to the category of incompletely restrained positioning mechanism (IRPMs) according to Ming and Higuchi [25]. For IRPMs, the mechanism cannot maintain its own rigidity and needs an external load to make all cables taut. Three types of external load are usually adopted.

The first type is gravity, which is used in most suspended cable-driven mechanisms. In this case, gravity is employed as a virtual cable whose tension force is always downwards. A representative example is the RoboCrane [13]. The second typical external force is the upward buoyancy force, which serves as a virtual cable providing upward force in the cable-driven balloon robot [27]. Aside from the natural gravity force and buoyancy force, there exists an artificial external force produced by the spine-like element between the moving platform and fixed base to keep the cables in tension [12]. The spine element can be a spring or a rigid kinematic chain. Our mechanism belongs to the first case using a spring as the spine element.

Although the idea of using a spring in a cable-driven mechanism is not new, the analysis for such a mechanism is scarce. In the iCub head design, the authors just list the cable-driven mechanism base on the spring spine without any analysis [6]. To the best of our knowledge, the only analysis for such a mechanism is presented in the James head design [8], where the inverse kinematics are obtained. The analysis, however, relies on assumptions of a constant spring length and a constant spring curvature, which cannot hold all the time. In fact, the deformation of the spring should be treated as a lateral buckling problem. The first analysis considering spring buckling is given by us in Ref. [1], where the statics are obtained. However, the derivation is for a simplified case when only two of the four cables are actuated simultaneously. Based on a spring lateral buckling model, this paper aims to give a general solution to the kinematics and statics when all the four cables are actuated independently. It will be shown that it is different from a traditional analysis with separate kinematics and statics; instead, we need to combine them together to obtain the results because the lateral buckling of spring [26]. Detailed main contributions of this paper are:

- General statics analysis of the compressive spring lateral buckling.
- Combined inverse position and statics analysis for the cable-driven parallel mechanism with a spring spine.
- Optimal placement of cables for the mechanism.

The rest of paper is organized as follows. In Section 2, descriptions of the mechanism including the notations used in this paper and the d.o.f. parametrization for the mechanism are presented. After that, the inverse position and statics are solved simultaneously in Section 3. Based on the statics, the optimal design for cable placements is performed in Section 4. Finally, conclusions are given in Section 5.

2. Description of the Mechanism

The general configuration of the mechanism analyzed in this paper is shown in Fig. 3. There are four main components of the mechanism:

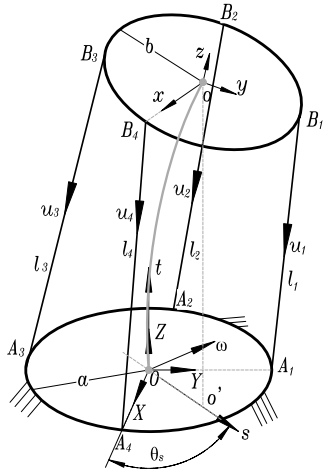

Figure 3. Schematic of the proposed parallel mechanism.

- *Fixed base*. This is the fixed part of the mechanism to which a fixed coordinate frame $OXYZ$ is attached. The origin of the frame is at the bottom center of the spring, the X-axis is along $\overrightarrow{OA_4}$, the Y-axis is along $\overrightarrow{OA_1}$ and the Z-axis is determined by the right-hand rule.

- *Moving platform*. This is the moving part of the mechanism, to which the head will be mounted. A body frame $oxyz$ is attached to this moving platform, with the origin o at the top center of the spring, the x-axis along $\overrightarrow{OB_4}$, the y-axis along $\overrightarrow{OB_1}$ and the z-axis determined by the right-hand rule.

- *Cables*. Four flexible cables with negligible mass and diameter are connected to the moving platform at point B_i $(i = 1, 2, 3, 4)$ and pulled from the fixed base at point A_i. Both A_i and B_i are equidistance to each other on the circle with radii $|OA_i| = a$ and $|oB_i| = b$ with respect to the center O and o, respectively. $\overrightarrow{OA_i}$ and $\overrightarrow{OB_i}$ are along the same direction in the initial configuration. Denote the force value along the cable as T_i, the cable length between A_i and B_i as l_i, and the unit vector for the direction of force in each cable as $\mathbf{u}_i$. We use bold letters to denote vectors (e.g., $T_i\mathbf{u}_i = \mathbf{T}_i$). Similar expressions are applied for other variables.

- *Spine*. The compression spring produces a force/torque between the fixed base and the moving platform to support the robot head and facilitate the head motion. It is shown as a curve from point O to point o in Fig. 3. Note that since the spring is rigidly connected to the fixed base at point O, the tangent vector for the spring curve at O is perpendicular to the fixed base plane. Similar arguments can be applied to point o and the moving platform plane.

Due to the symmetric placements of cables, we can assume the spring will bend in a plane. Moreover, since the torsional strength for spring compression is quite

large, we also assume the moving platform cannot rotate about the z-axis of the body frame $oxyz$. As these two assumptions will be frequently referred to later, we state them as one assumption:

Assumption 1. The spring curve is always in a plane and the moving platform cannot rotate about the z-axis.

The plane for the spring curve, shown in Fig. 3, is formed by O, o and o', where o' is the vertical projection of o onto the fixed base. In this plane, a planar body frame Ost is attached to this spring. The origin is the same as the fixed frame $OXYZ$, the t-axis is the same as the Z-axis in frame $OXYZ$ and the s-axis is along $\overrightarrow{Oo'}$. Under Assumption 1, we need four parameters to define the configuration of the moving platform:

θ_s angle between axis s and axis X (bending direction).

θ_p angle between the fixed base plane and the moving platform plane (bending amplitude).

t_0 t coordinate for point o in the spring attached frame Ost (vertical length of the bending spring).

s_0 s coordinate for point o in frame Ost (lateral translation for the bending spring).

Note that other parameter sets can also be used to describe the moving platform's configuration, but the above parametrization is most suitable for human head movement. However, we cannot arbitrarily assign the values for those four parameters. In fact, there are only three independent parameters among them. Without loss of generality, we can consider s_0 to be the dependent parameter. In other words, once θ_s, θ_p and t_0 are given, s_0 can be solved. In this case, s_0 is considered as a parasitic motion that can be determined by the other three parameters. This parasitic motion is frequently encountered in parallel manipulators [28]. As defined by the IFToMM, the d.o.f. is the number of independent coordinates needed to define the configuration of a mechanism [29]. According to this definition, this mechanism has only 3 d.o.f.

The homogeneous coordinates of A_i in the fixed base with respect to the frame $OXYZ$ can be described as:

$$
\begin{aligned}
{}^{O}\mathbf{a}_1 &= (0, a, 0, 1)^{\mathrm{T}}, \quad {}^{O}\mathbf{a}_2 = (-a, 0, 0, 1)^{\mathrm{T}} \\
{}^{O}\mathbf{a}_3 &= (0, -a, 0, 1)^{\mathrm{T}}, \quad {}^{O}\mathbf{a}_4 = (a, 0, 0, 1)^{\mathrm{T}}.
\end{aligned}
$$

Similarly, the homogeneous coordinates of B_i in the moving platform with respect to $oxyz$ are:

$$
\begin{aligned}
{}^{o}\mathbf{b}_1 &= (0, b, 0, 1)^{\mathrm{T}}, \quad {}^{o}\mathbf{b}_2 = (-b, 0, 0, 1)^{\mathrm{T}} \\
{}^{o}\mathbf{b}_3 &= (0, -b, 0, 1)^{\mathrm{T}}, \quad {}^{o}\mathbf{b}_4 = (b, 0, 0, 1)^{\mathrm{T}}.
\end{aligned}
$$

The rotational matrix from the body frame to the fixed frame can be considered as the rotation about an axis $\boldsymbol{\omega}$ perpendicular to Os with an angle θ_p, where $\boldsymbol{\omega} = [-\sin\theta_s, \cos\theta_s, 0]^{\mathrm{T}}$ is shown in Fig. 3. Using Rodrigues' formula, the rotational matrix can be obtained as:

$$^{O}\mathbf{R}_o = \mathrm{e}^{\widehat{\boldsymbol{\omega}}\theta_p} = \mathbf{I} + \widehat{\boldsymbol{\omega}}\sin\theta_p + \widehat{\boldsymbol{\omega}}^2(1-\cos\theta_p) = \begin{pmatrix} t_{11} & t_{12} & t_{13} \\ t_{21} & t_{22} & t_{23} \\ t_{31} & t_{32} & t_{33} \end{pmatrix},$$

where $\widehat{\boldsymbol{\omega}}$ is the skew symmetric matrix generated by $\boldsymbol{\omega}$, $\mathbf{I}$ is the identity matrix and:

$$\begin{aligned} t_{11} &= \sin^2\theta_s + \cos\theta_p\cos^2\theta_s, & t_{12} &= t_{21} = (\cos\theta_p - 1)\cos\theta_s\sin\theta_s \\ t_{13} &= \sin\theta_p\cos\theta_s, & t_{22} &= \cos^2\theta_s + \cos\theta_p\sin^2\theta_s \\ t_{23} &= \sin\theta_p\sin\theta_s, & t_{31} &= -\sin\theta_p\cos\theta_s \\ t_{32} &= -\sin\theta_p\sin\theta_s, & t_{33} &= \cos\theta_p. \end{aligned}$$

Then the homogeneous transformation matrix is:

$$^{O}\mathbf{T}_o = \begin{pmatrix} t_{11} & t_{12} & t_{13} & s_0\cos\theta_s \\ t_{21} & t_{22} & t_{23} & s_0\sin\theta_s \\ t_{31} & t_{22} & t_{33} & t_0 \\ 0 & 0 & 0 & 1 \end{pmatrix}.$$

3. Combined Inverse Position and Statics Analysis

For the inverse position analysis, we want to obtain the driven cable length given the desired d.o.f. value. Let $\mathbf{x} = [\theta_s, \theta_p, t_0]^{\mathrm{T}} \in \mathbb{R}^3$ and $\mathbf{q} = [l_1, l_2, l_3, l_4]^{\mathrm{T}} \in \mathbb{R}^4$, the inverse position is to find the relation:

$$\mathbf{q} = f(\mathbf{x}), \quad f : \mathbb{R}^3 \to \mathbb{R}^4.$$

If s_0 is solved from $\mathbf{x}$, then $^{O}\mathbf{T}_o$ is completely determined and the cable lengths can be easily solved from $l_i = \| ^{O}\mathbf{T}_o {}^{o}\mathbf{b}_i - {}^{O}\mathbf{a}_i \|$ $(i = 1, 2, 3, 4)$. Nevertheless, s_0 cannot be arbitrarily assigned. This parasitic motion is a characteristic of the spring buckling, which is caused by the forces acting on the spring. These forces mainly result from the pulling forces in the four cables and the mass of the payload. Therefore, we should combine the inverse position and statics in order to obtain a solution. The general procedure is:

(i) Transform all the cable forces to the equivalent force and moment applied at the spring's top center.

(ii) Use the equivalent force and moment to get the desired spring lateral buckling equations.

(iii) Solve s_0.

(iv) Solve the inverse position and statics.

These steps are elaborated in the following two subsections.

3.1. Force and Moment Balance Equations

With Assumption 1, all the cable forces can be transformed into bending plane Ost; otherwise, the spring will not bend in that plane. In other words, we can convert all the forces to two perpendicular forces F_1 and F_2 in the plane, and a moment M perpendicular to the plane at the spring's top center as shown in Fig. 4. Without loss of generality, we assume the moving platform is not subject to external forces. The case when there are external forces such as the weight of the respirators can be analyzed in the same way. The mass of the moving platform is taken as a mass point at the spring's top center with quantity m. For the force and moment balance, we have:

$$\sum_{i=1}^{4} T_i {}^{O}\mathbf{u}_i + [0,\ 0,\ -mg]^{\mathrm{T}} = [F_1 \cos\theta_s,\ F_1 \sin\theta_s, -F_2]^{\mathrm{T}} \tag{1}$$

$$\sum_{i=1}^{4} {}^{O}\mathbf{r}_i \times T_i {}^{O}\mathbf{u}_i = [-M \sin\theta_s,\ M \cos\theta_s,\ 0]^{\mathrm{T}}, \tag{2}$$

where ${}^{O}\mathbf{u}_i = ({}^{O}\mathbf{a}_i - {}^{O}\mathbf{T}_o {}^{o}\mathbf{b}_i)/\|{}^{O}\mathbf{a}_i - {}^{O}\mathbf{T}_o {}^{o}\mathbf{b}_i\|$ and ${}^{O}\mathbf{r}_i$ corresponds to the vector $\overrightarrow{oB_i}$ expressed in the fixed frame:

$$
\begin{aligned}
{}^{O}\mathbf{r}_1 &= b[t_{12},\ t_{22},\ t_{32}]^{\mathrm{T}}, \qquad {}^{O}\mathbf{r}_2 = b[-t_{11},\ -t_{21},\ -t_{31}]^{\mathrm{T}} \\
{}^{O}\mathbf{r}_3 &= b[-t_{12},\ -t_{22},\ -t_{32}]^{\mathrm{T}}, \qquad {}^{O}\mathbf{r}_4 = b[t_{11},\ t_{21},\ t_{31}]^{\mathrm{T}}.
\end{aligned}
$$

In (1) and (2), there are in total eight unknowns: T_1 to T_4, F_1, F_2, M and s_0. We will show that T_1 to T_4 can be eliminated, and an equation with only F_1, F_2, M and s_0 as the unknowns can be obtained. This equation can be combined with another three equations from the spring's lateral buckling to solve the four unknowns. To simplify the notations, let $F_2' = F_2 - mg$. Equations (1) and (2) can be decomposed

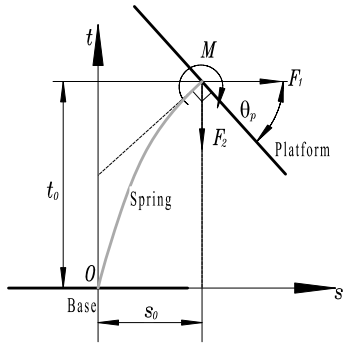

Figure 4. Bending plane equivalent force system.

into six equations:

$$s_0\cos\theta_s\left(T_1'+T_2'+T_3'+T_4'\right)+\left(T_2'-T_4'\right)(a-t_{11}b)+\left(T_1'-T_3'\right)t_{12}b+F_1\cos\theta_s=0 \tag{3}$$

$$s_0\sin\theta_s\left(T_1'+T_2'+T_3'+T_4'\right)-\left(T_1'-T_3'\right)(a-t_{22}b)-\left(T_2'-T_4'\right)t_{21}b+F_1\sin\theta_s=0 \tag{4}$$

$$b\left[\left(T_1'-T_3'\right)t_{32}-\left(T_2'-T_4'\right)t_{31}\right]+t_0\left(T_1'+T_2'+T_3'+T_4'\right)-F_2'=0 \tag{5}$$

$$\left(T_1'-T_3'\right)(t_{22}t_0-t_{32}s_0\sin\theta_s)+\left(T_1'+T_3'\right)at_{32}+\left(T_2'-T_4'\right)(t_{31}s_0\sin\theta_s-t_{21}t_0)-\frac{M}{b}\sin\theta_s=0 \tag{6}$$

$$\left(T_2'-T_4'\right)(t_{11}t_0-t_{31}s_0\cos\theta_s)-\left(T_2'+T_4'\right)at_{31}+\left(T_1'-T_3'\right)(t_{32}s_0\cos\theta_s-t_{12}t_0)+\frac{M}{b}\cos\theta_s=0 \tag{7}$$

$$s_0\left[\left(T_1'-T_3'\right)\cos\theta_s+\left(T_2'-T_4'\right)\sin\theta_s\right]+a(\cos\theta_p-1)\sin\theta_s\cos\theta_s\left[\left(T_1'+T_3'\right)-\left(T_2'+T_4'\right)\right]=0, \tag{8}$$

where $T_i'=T_i/l_i$. From (3) $\times\sin\theta_s-(4)\times\cos\theta_s$, we have:

$$(a-b)\left[\left(T_1'-T_3'\right)\cos\theta_s+\left(T_2'-T_4'\right)\sin\theta_s\right]=0. \tag{9}$$

From (6) $\times\cos\theta_s+(7)\times\sin\theta_s$, we have:

$$t_0\left[\left(T_1'-T_3'\right)\cos\theta_s+\left(T_2'-T_4'\right)\sin\theta_s\right]-a\sin\theta_p\sin\theta_s\cos\theta_s\left[\left(T_1'+T_3'\right)-\left(T_2'+T_4'\right)\right]=0. \tag{10}$$

From (8) $\times\sin\theta_p-(10)\times(1-\cos\theta_p)$, we have:

$$\left[t_0(\cos\theta_p-1)+s_0\sin\theta_p\right]\left[\left(T_1'-T_3'\right)\cos\theta_s+\left(T_2'-T_4'\right)\sin\theta_s\right]=0. \tag{11}$$

Assume $a\neq b$ or $t_0(\cos\theta_p-1)+s_0\sin\theta_p\neq 0$ (the case when $a=b$ and $t_0(\cos\theta_p-1)+s_0\sin\theta_p=0$ will be treated as a special case later). Then, (9) and (11) are of the same form:

$$\left(T_1'-T_3'\right)\cos\theta_s+\left(T_2'-T_4'\right)\sin\theta_s=0. \tag{12}$$

Substitute (12) into (10). Since $a\neq 0$ and $\sin\theta_p\neq 0$ for small $\theta_p\neq 0$, we have:

$$T_2'+T_4'=T_1'+T_3', \tag{13}$$

provided $\theta_s\neq\frac{k\pi}{2}$, $k=0,1,2,\ldots$ (the case when $\theta_s=\frac{k\pi}{2}$ will be treated as another special case later). Substitute (12) and (13) into (3), (5) and (6); three new equations can be obtained:

$$2s_0\sin\theta_s\left(T_1'+T_3'\right)+(b\cos\theta_p-a)\left(T_1'-T_3'\right)+F_1\sin\theta_s=0$$

$$2t_0\sin\theta_s\left(T_1'+T_3'\right)-b\sin\theta_p\left(T_1'-T_3'\right)-F_2'\sin\theta_s=0$$

$$a\sin\theta_p\sin\theta_s\left(T_1'+T_3'\right)-(t_0\cos\theta_p+s_0\sin\theta_p)\left(T_1'-T_3'\right)+\frac{M}{b}\sin\theta_s=0.$$

From the first two equations, we can solve for $T_1' - T_3'$ and $T_1' + T_3'$ as:

$$T_1' - T_3' = \frac{\sin\theta_s(t_0 F_1 + s_0 F_2')}{t_0(a - b\cos\theta_p) - b s_0 \sin\theta_p} \tag{14}$$

$$T_1' + T_3' = \frac{F_1 b \sin\theta_p + F_2'(a - b\cos\theta_p)}{2t_0(a - b\cos\theta_p) - 2b s_0 \sin\theta_p}. \tag{15}$$

Substituting these two equations to the third equation to eliminate T_1' and T_3', we have:

$$\begin{aligned} &2bF_2' \sin\theta_p s_0^2 + 2b\big(t_0 F_1 \sin\theta_p + M\sin\theta_p + t_0 F_2' \cos\theta_p\big)s_0 \\ &\quad + \big(2bt_0^2 \cos\theta_p - ab^2 \sin^2\theta_p\big)F_1 - ab\sin\theta_p(a - b\cos\theta_p)F_2' \\ &\quad - 2t_0(a - b\cos\theta_p)M = 0. \end{aligned} \tag{16}$$

In this equation, the unknown variables are F_1, F_2', M and s_0. In the next subsection, we will show that F_2' can be obtained through t_0, while F_1 and M can be expressed as a linear function of s_0 from the spring's lateral buckling equation. In this way, we can solve (16) for s_0 and all the other unknown variables can be obtained.

3.2. Lateral Buckling Equations for the Spring

The spring buckling problem was first investigated by Timoshenko — the father of modern engineering mechanics. He derived the rigidity of the compression, lateral and shear deflections for a coil spring to explain the stability bounds of a compressed helical spring due to buckling [30]. The same results were also concluded by Wahl in 1963 [31]. Timoshenko [30] also pointed out that the lateral buckling of a coil compression spring could be treated using the same methods as elastic bars, but it was necessary to consider the change in length of the spring due to compression since the change was not negligible as in the case of compressed bars. We will follow this suggestion to analyze the spring buckling problem.

Assume the notations of the selected compression helical spring are as follows: K is the spring constant, l_0 is the initial length, h_0 is the pitch, n is the number of coils, r is the radius, t_0 is the vertical length after compression, β_0 is the flexural rigidity that corresponds to the same physical meaning for the solid bar and β is the same quantity after compression. For β and β_0, we have:

$$\beta = \beta_0 \frac{t_0}{l_0} \quad \text{and} \quad \beta_0 = \frac{2EGIh_0}{\pi r(E + 2G)},$$

where E is the elastic modulus, G is the shearing modulus and I is the moment of inertia of the cross-section of the spring wire with respect to its diameter [30].

Since the spring's compression length is usually small after compression, we can neglect the length reduction resulting from the lateral buckling and approximate F_2 using Hooke's law:

$$F_2 = K(l_0 - t_0). \tag{17}$$

We take the spring as a flexible bar to investigate lateral buckling characteristics of the spring [30]. Consider the situation shown in Fig. 4. The spring will be buckled by forces F_1 and F_2 plus a couple M. For any cross-section of the spring, the following equation is satisfied for its deformation:

$$\beta \frac{\mathrm{d}^2 s/\mathrm{d}t^2}{[1+(\mathrm{d}s/\mathrm{d}t)^2]^{3/2}} = M + F_2(s_0 - s) + F_1(t_0 - t). \tag{18}$$

The right-hand side is the total moment applied to a cross-section of the spring. This equation does not have an analytical solution, but the numerical solution can be obtained by calculating elliptic integrals [32]. For small deflection, the above equation can be simplified to a linear case:

$$\beta \frac{\mathrm{d}^2 s}{\mathrm{d}t^2} = M + F_2(s_0 - s) + F_1(t_0 - t). \tag{19}$$

The solution for this equation is:

$$s = C_1 \cos\left(\sqrt{F_2/\beta}t\right) + C_2 \sin\left(\sqrt{F_2/\beta}t\right) - \frac{F_1}{F_2}t + \frac{M + F_2 s_0 + F_1 t_0}{F_2}, \tag{20}$$

where $C_1 = -(M + F_2 s_0 + F_1 t_0)/F_2$ and $C_2 = F_1\sqrt{\beta}/F_2^{3/2}$ are constants obtained from two initial conditions for the built-in end connecting to the fixed base: $s(0) = 0$, $s'(0) = 0$. Substituting the other two initial conditions for the free end connecting to the moving platform: $s(t_0) = s_0$, $s'(t_0) = \tan\theta_p$ to (20), we can obtain another two equations:

$$-(M + F_2 s_0 + F_1 t_0)\cos\left(\sqrt{F_2/\beta}t_0\right) + F_1\sqrt{\beta/F_2}\sin\left(\sqrt{F_2/\beta}t_0\right) + M = 0$$
$$\sqrt{F_2/\beta}(M + F_2 s_0 + F_1 t_0)\sin\left(\sqrt{F_2/\beta}t_0\right) + F_1\cos\left(\sqrt{F_2/\beta}t_0\right) - F_1 - F_2\tan\theta_p = 0,$$

which can be rewritten as:

$$a_1 M + b_1 F_1 + c_1 s_0 + d_1 = 0 \tag{21}$$
$$a_2 M + b_2 F_1 + c_2 s_0 + d_2 = 0, \tag{22}$$

where:

$$a_1 = 1 - \cos\left(\sqrt{F_2/\beta}t_0\right), \qquad b_1 = \sqrt{\beta/F_2}\sin\left(\sqrt{F_2/\beta}t_0\right) - t_0\cos\left(\sqrt{F_2/\beta}t_0\right)$$
$$c_1 = -F_2\cos\left(\sqrt{F_2/\beta}t_0\right), \qquad d_1 = 0$$
$$a_2 = \sqrt{F_2/\beta}\sin\left(\sqrt{F_2/\beta}t_0\right), \qquad b_2 = \cos\left(\sqrt{F_2/\beta}t_0\right) + t_0\sqrt{F_2/\beta}\sin\left(\sqrt{F_2/\beta}t_0\right) - 1$$
$$c_2 = F_2\sqrt{F_2/\beta}\sin\left(\sqrt{F_2/\beta}t_0\right), \qquad d_2 = -F_2\tan\theta_p.$$

These two equations are linear equations of M, F_1 and s_0, where all the coefficients are known. Therefore, we can express M and F_1 as a function of s_0:

$$F_1 = D_1 s_0 + E_1 \tag{23}$$
$$M = D_2 s_0 + E_2, \tag{24}$$

where:

$$D_1 = -\frac{a_2c_1 - a_1c_2}{a_2b_1 - a_1b_2}, \qquad E_1 = -\frac{a_2d_1 - a_1d_2}{a_2b_1 - a_1b_2}$$
$$D_2 = -\frac{b_2c_1 - b_1c_2}{b_2a_1 - b_1a_2}, \qquad E_2 = -\frac{b_2d_1 - b_1d_2}{b_2a_1 - b_1a_2}.$$

Plugging (23) and (24) to (16), we can get a quadratic equation of s_0:

$$As_0^2 + Bs_0 + C = 0, \tag{25}$$

where:

$$A = 2b\sin\theta_p\left(F_2' + t_0D_1 + D_2\right)$$
$$B = 2bt_0\left(F_2'\cos\theta_p + E_1\sin\theta_p\right) + 2bE_2\sin\theta_p + \left(2bt_0^2\cos\theta_p - ab^2\sin^2\theta_p\right)D_1 - 2t_0(a - b\cos\theta_p)D_2$$
$$C = \left(2bt_0^2\cos\theta_p - ab^2\sin^2\theta_p\right)E_1 - ab\sin\theta_p(a - b\cos\theta_p)F_2' - 2t_0(a - b\cos\theta_p)E_2.$$

Denote the set of nonnegative real numbers as $\mathbb{R}_{\geqslant 0}$, then we need to find $s_0 \in \mathbb{R}_{\geqslant 0}$. Once s_0 is obtained, all the other unknowns can be solved. Note that we have nine equations, (3)–(8), (17), (21) and (22), to solve eight unknowns (T_1–T_4, F_1, F_2, M and s_0). Generally, there is no solution because the number of equations is larger than the number of unknowns; however, since (9) and (11) are the same if the conditions stated before hold, there are only eight equations for eight unknowns.

Remark 1. According to Ming and Higuchi [25], only n cables are needed to obtain n d.o.f. for an IRPM with the help of external force. Therefore, we may only need three cables to actuate the mechanism. The reason we use four cables is based on our previous implementation [1]. However, it would be interesting to see what will happen if there are only three actuated cables, such as the James humanoid head [8] and the first parallel manipulator of the iCub head design [6].

Remark 2. The above procedures does not consider the constraint that $T_i \in \mathbb{R}_{\geqslant 0}$, $\forall i$. At certain posture, it may occur that some $T_i < 0$. In this case, the posture is not feasible. Therefore, a wrench feasible workspace [18, 19, 21] analysis is necessary. The analysis for the spring-based mechanism, however, relies on the nonlinear version of the buckling equation because the linear one is only an approximation. We will not provide such an analysis in this paper.

Remark 3. From the above derivation, we can also see that s_0 cannot be assigned arbitrarily because (25) should be satisfied. Therefore, only the other three parameters θ_s, θ_p and t_0 can be assigned arbitrarily, and the mechanism has only 3 d.o.f. Note that, however, we can choose other parameters (θ_s, θ_p or t_0) instead of s_0 to be the parasitic motion and a similar derivation procedure can be performed.

3.3. Special Cases

In the above derivation, we have made the assumptions $a \neq b$ or $t_0(\cos\theta_p - 1) + s_0 \sin\theta_p \neq 0$ to obtain (12), and $\theta_s \neq \frac{k\pi}{2}$ and $k = 0, 1, 2, \ldots$, to obtain (13). In this subsection, we will discuss these special cases.

3.3.1. $(T_1' - T_3')\cos\theta_s + (T_2' - T_4')\sin\theta_s \neq 0$
If $(T_1' - T_3')\cos\theta_s + (T_2' - T_4')\sin\theta_s \neq 0$, we have both $a = b$ and $t_0(\cos\theta_p - 1) + s_0 \sin\theta_p = 0$, and the latter equation can be simplified as $s_0/t_0 = \tan(\theta_p/2)$. However, we will show that if $a = b$, then $s_0/t_0 = \tan(\theta_p/2)$ only when $\theta_p = 0$. This means we will always have $(T_1' - T_3')\cos\theta_s + (T_2' - T_4')\sin\theta_s = 0$ provided $\theta_p \neq 0$.

In fact, under the condition of $a = b$, the three decomposed equations for (1) are:

$$\begin{aligned}
&\cos\theta_s\big\{s_0\big(T_1' + T_2' + T_3' + T_4'\big) \\
&\quad + a(1 - \cos\theta_p)\big[\big(T_2' - T_4'\big)\cos\theta_s - \big(T_1' - T_3'\big)\sin\theta_s\big] + F_1\big\} = 0 \qquad (26)\\
&\sin\theta_s\big\{s_0\big(T_1' + T_2' + T_3' + T_4'\big) \\
&\quad + a(1 - \cos\theta_p)\big[\big(T_2' - T_4'\big)\cos\theta_s - \big(T_1' - T_3'\big)\sin\theta_s\big] + F_1\big\} = 0 \qquad (27)\\
&\quad t_0\big(T_1' + T_2' + T_3' + T_4'\big) \\
&\qquad + a\sin\theta_p\big[\big(T_2' - T_4'\big)\cos\theta_s - \big(T_1' - T_3'\big)\sin\theta_s\big] - F_2' = 0. \qquad (28)
\end{aligned}$$

Note that (26) and (27) are the same if $\theta_s \neq \frac{k\pi}{2}$.

If $s_0/t_0 = \tan(\theta_p/2)$, then from (27) and (28), we have $F_1 t_0 + F_2' s_0 = 0$ that, combined with (21) and (22), can be used to obtain another expression of s_0:

$$s_0' = \frac{a_1 d_2 - a_2 d_1}{a_2(c_1 - b_1 F_2'/t_0) - a_1(c_2 - b_2 F_2'/t_0)} = \frac{a_1 d_2 - a_2 d_1}{a_2(t_0 c_1 - b_1 F_2') - a_1(t_0 c_2 - b_2 F_2')}.$$

We can rewrite it by substituting the expressions for a_1, a_2, b_1, b_2, c_1, c_2, d_1 and d_2:

$$\frac{s_0'}{t_0} = \frac{[\cos(\sqrt{F_2/\beta}\,t_0) - 1]F_2 \tan\theta_p}{2(F_2 - mg)[\cos(\sqrt{F_2/\beta}\,t_0) - 1] - mgt_0\sqrt{F_2/\beta}\sin(\sqrt{F_2/\beta}\,t_0)}.$$

We expect $s_0' = s_0$ so that $s_0'/t_0 = s_0/t_0$; however, this is only valid when $\theta_p = 0$. An analytical verification is difficult, but we can use the numerical approach to see the relation. Since we will assume t_0 is fixed in the following sections, we can plot the three-dimensional (3-D) graph with fixed t_0, and using θ_s and θ_p as the x and y coordinates and $s_0'/t_0 - s_0/t_0$ as the z coordinate. The diagram for $t_0 = 0.085$ m, $a = b = 0.05$ m, $\theta_s \in [0, 2\pi)$ and $\theta_p \in [0, \pi/9]$ is shown in Fig. 5. From Fig. 5, we see that $s_0'/t_0 - s_0/t_0$ is strictly monotonically increasing with respect to θ_p and the only case for $s_0'/t_0 = s_0/t_0$ is when $\theta_p = 0$. As the case for $\theta_p = 0$ is not interesting as there is no bending motion of the head, we will assume $\theta_p \neq 0$ in the following to avoid this special case and ensure $(T_1' - T_3')\cos\theta_s + (T_2' - T_4')\sin\theta_s = 0$ always hold.

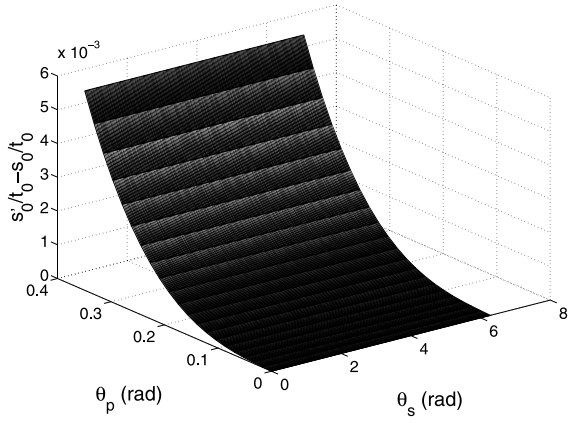

Figure 5. Difference between s_0'/t_0 and s_0/t_0 (vertical axis represents $s_0'/t_0 - s_0/t_0$).

3.3.2. $\theta_s = \frac{k\pi}{2}$, $k = 0, 1, 2, \ldots$

Without loss of generality, suppose $\theta_s \in [0, 2\pi)$, then there exist four special cases corresponding to $\theta_s = 0$, $\pi/2$, π or $3\pi/2$. We will give the detailed derivation for $\theta_s = 0$, and for the other three cases, both the procedure and results are the same.

When $\theta_s = 0$, (4), (6) and (8) all degenerate to $T_1' = T_3'$, and the other three equations for force and moment balance become:

$$s_0\left(T_1' + T_2' + T_3' + T_4'\right) + \left(T_2' - T_4'\right)(a - b\cos\theta_p) + F_1 = 0$$
$$t_0\left(T_1' + T_2' + T_3' + T_4'\right) + \left(T_2' - T_4'\right)b\sin\theta_p - F_2 = 0$$
$$a\sin\theta_p\left(T_2' + T_4'\right) + \left(T_2' - T_4'\right)(t_0\cos\theta_p + s_0\sin\theta_p) + M/b = 0.$$

Combining the other three equations from spring buckling, we cannot get a unique solution because there are only seven equations for eight unknowns. The reason is that we can have infinitely many values for T_1' and T_3' provided that they are equal. Therefore, we can force the value to satisfy:

$$T_1' + T_3' = T_2' + T_4',$$

to make it compatible to the analysis for non-special cases. In this way, eliminating T_1', T_2', T_3' and T_4', we can get the same equation as (16). Therefore, the solution for non-special cases can also be used to derive the solution for the special case when $\theta_s = \frac{k\pi}{2}$, $k = 0, 1, 2, \ldots$.

3.4. Numerical Implementations

The inverse position and statics analysis is implemented in MATLAB. Parameters of spring compression for the prototype are shown in Table 1, where d is the diameter of the spring wire. Therefore, we can get the following other parameters of the spring:

$$I = \frac{\pi d^4}{64} = 9.811 \times 10^{-12}\ \mathrm{m}^4, \qquad \beta_0 = \frac{2EGIh_0}{\pi r(E + 2G)} = 0.2321.$$

Table 1.
Parameters of selected compressed coil spring

l_0 (m)	h_0 (m)	G (GPa)	E (GPa)	r (m)	d (m)	K (N/m)
0.1016	0.0195	81.2	196.5	22.73×10^{-3}	3.76×10^{-3}	4153

Material: spring-tempered steel.

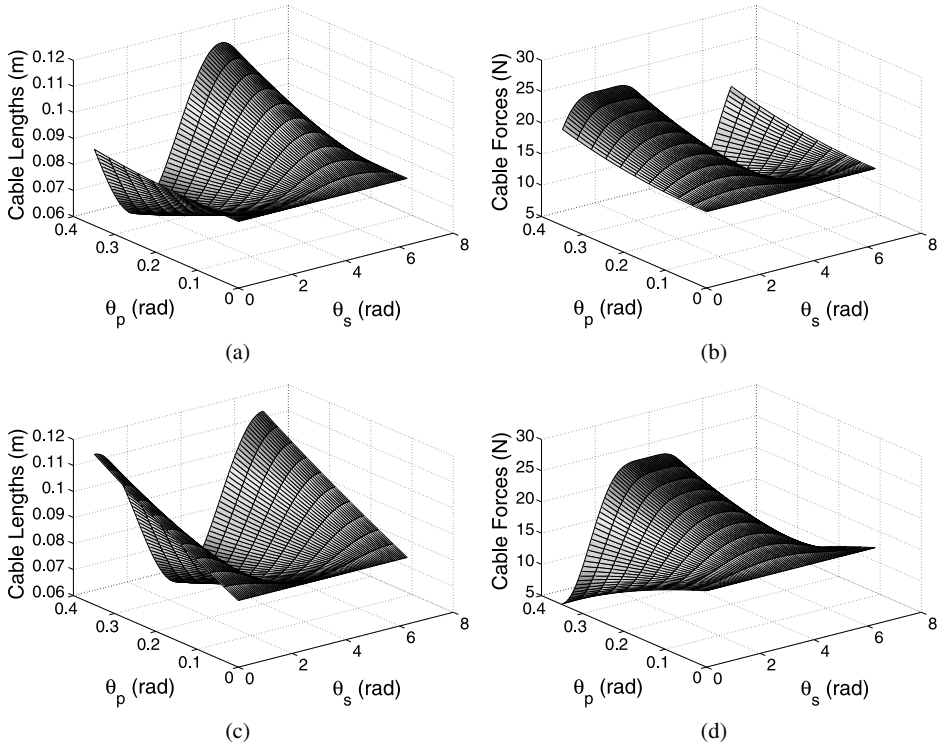

Figure 6. Inverse position and statics solution illustration (vertical axes are the cable lengths for the first column and cable forces for the second column). (a) L_1. (b) T_1. (c) L_2. (d) T_2. (e) L_3. (f) T_3. (g) L_4. (h) T_4.

The other parameters are chosen as $a = 0.06$ m, $b = 0.05$ m and $m = 0.05$ kg. The implementation is performed with a fixed $t_0 = 0.085$ m because in real applications t_0 can only be used to adjust the pretension force in the four cables. By varying θ_p from 0 to $\pi/9$ and θ_s from 0 to 2π, we can obtain the results shown in Fig. 6, where the cables lengths and forces are shown as the z coordinate.

We can have three observations from Fig. 6. First of all, the length and force complement each other for each cable. In other words, when the length is small, the force will be large. This is in accordance with our intuition because when the cable length is small, the cable should exert a large force on the moving platform.

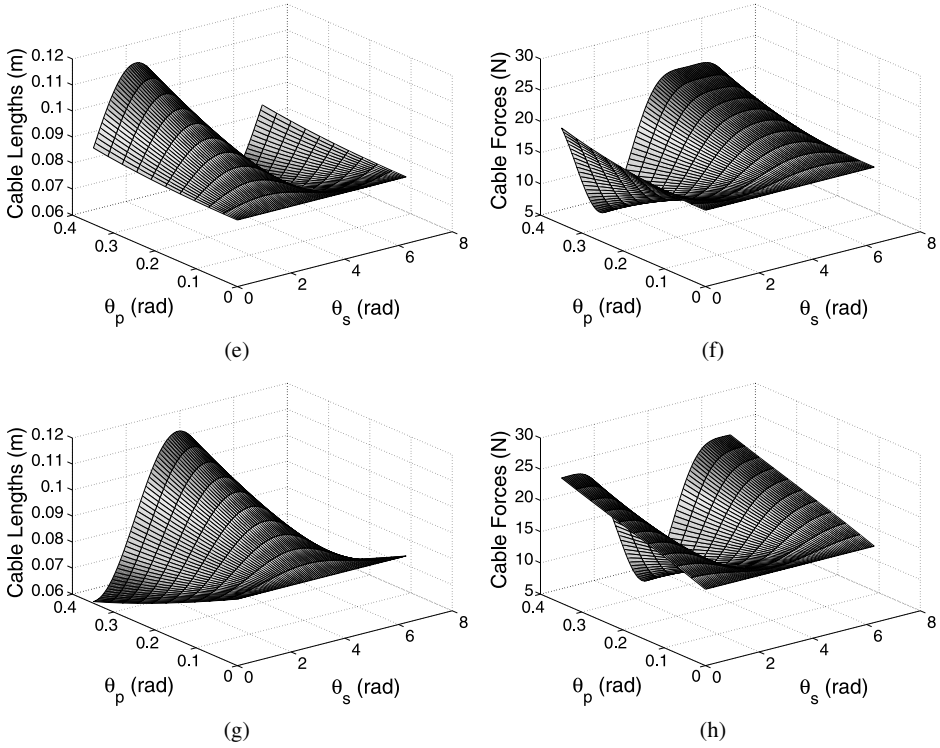

Figure 6. (Continued.)

The second observation from Fig. 6 is that when θ_p is large, the variations of both the force and length are also large. This is because the more we want to bend the moving platform, the larger force we need to act on it. Finally, for a fixed θ_p, the length and force curves for all the cables with θ_s from 0 to 2π are symmetric. This cannot be seen clearly from Fig. 6; therefore, we plot all the cable lengths and forces with $\theta_s = \pi/9$ and $t_0 = 0.085$ m in Fig. 7a and b, respectively. It is clear that all the curves have the same profile, but with different phases.

4. Optimal Placement of Cables

Based on the combined inverse position and statics analysis, we can perform an optimal design to obtain the minimum actuation force to decrease the size of actuators and reduce cost. For such a goal, the optimization variables should be first identified. From the force equations (14) and (15) in Section 3, the optimization variables should be a and b, which represent the cables' end positions at the fixed base and moving platform, because all other variables should either be specified (θ_s, θ_p and t_0) or solved (s_0, F_1 and F_2'). Although there is research on optimally assigning the tension forces among all the cables in redundant cable-driven manipulators [22, 23], the research on how to optimally choose the connecting point is seldom discussed.

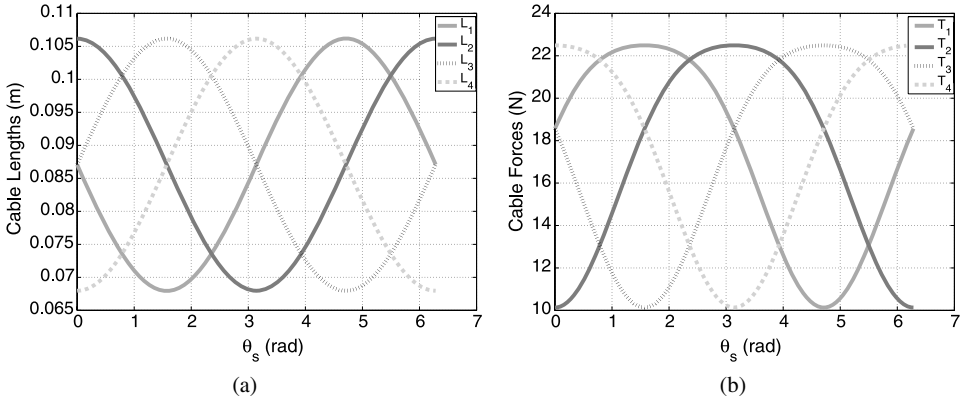

(a) (b)

Figure 7. Inverse position and statics with $\theta_s = \pi/9$ and $t_0 = 0.085$ m. (a) Cable lengths for θ_s from 0 to 2π. (b) Cable forces for θ_s from 0 to 2π.

In this section, we will use the numerical approach to obtain optimal a and b based on different objective functions.

Since there are four cable forces in total, we need to define a proper measure to evaluate the overall force magnitude. Two different measures can be defined:

- Total forces: $T_{\text{sum}} = \sum_{i=1}^{4} |T_i|$.
- Maximum force: $T_{\max} = \max\{|T_1|, |T_2|, |T_3|, |T_4|\}$.

These two measures are chosen because they represent the average and maximum control effort from the motors, respectively. Note that the cable forces are non-negative because the single directional actuation ability for cables. As a result, the absolute value symbols can be dropped in the above definition. Moreover, since the type of measure should be clear from the context, we will also drop the subscript and use T to represent the above two measures in the following discussion.

T is a function of θ_s, θ_p, t_0, a and b. Without loss of generality, we can fix t_0 because different t_0 can be obtained by pretightening all the four cables simultaneously. Therefore, we assume $t_0 = 0.085$ m in the following optimization. In this case, we can write:

$$T = \delta(\theta_s, \theta_p, a, b), \quad \delta : \mathbb{R}^4 \to \mathbb{R}.$$

Note that an analytical expression for T is available because expression for individual T_i can be obtained. We illustrate the idea for T_1. In fact, $T_1 = T_1' l_1$, where T_1' can be obtained from (14) and (15) as:

$$T_1' = \frac{(2t_0 \sin\theta_s + b\sin\theta_p)F_1 + (2s_0 \sin\theta_s + a - b\cos\theta_p)F_2'}{4(t_0(a - b\cos\theta_p) - bs_0 \sin\theta_p)},$$

where $F_1 = D_1 s_0 + E_1$ and $F_2' = F_2 - mg = K(l_0 - t_0) - mg$. If we plug the analytical solution of s_0 from (25) to the above equation, then we can obtain the expression for T_1'. Similar arguments can be applied to l_1. Therefore, there exists an

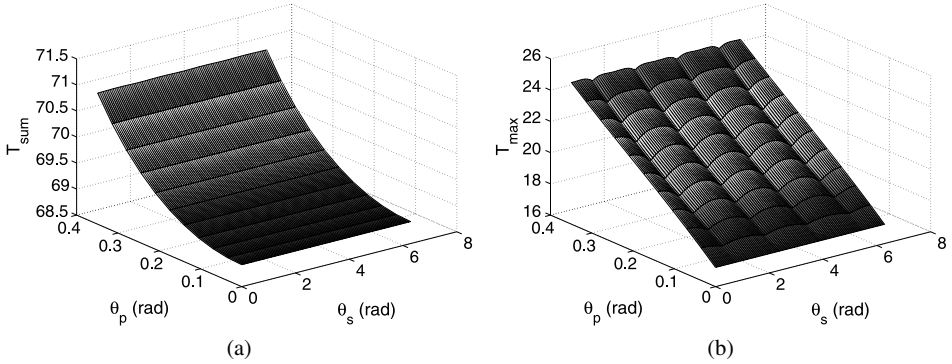

Figure 8. Variation of T when $t_0 = 0.085$, $a = 0.06$ and $b = 0.05$ m (vertical axes represent forces). (a) T_{sum}. (b) $T_{\max}$.

analytical expression for T_i, which leads to an analytical expression for T. The final expression for T, however, will be very complicated as we can see from T_1. As a result, we will not try to use the analytical approach to derive the optimal solution; instead, we will use the iterative numerical method.

Figure 8 shows the variation of T as a function of θ_s and θ_p when $a = 0.06$ m and $b = 0.05$ m. With different a and b, we can obtain different figures similar to Fig. 8. The goal is to find optimal a and b such that the resulting figure has the desired property such as the maximum value for T in the figure is minimum among all possible figures. In other words, we need to define an optimization objective function to encode the figure's desired property. This objective function should be a scalar function of only a and b. Denote such function as $g(a, b)$, $g : \mathbb{R}^2 \to \mathbb{R}$, then the minimization problem can be generally stated as:

$$\begin{aligned} &\text{minimize } g(a, b) \\ &\text{subject to } a_l \leqslant a \leqslant a_{\text{u}}, b_l \leqslant b \leqslant b_{\text{u}} \text{ and } T_i \geqslant 0 \ \ (i = 1, 2, 3, 4), \end{aligned} \tag{29}$$

where a_l, a_{u}, b_l and b_{u} are the lower bound and upper bound for a and b, respectively, which can be derived from the size of the human neck and the outer diameter of the spring. In the following, we let $a_l = b_l = 0.03$ m and $a_{\text{u}} = b_{\text{u}} = 0.08$ m. $T_i \geqslant 0$ is the condition that the forces in the cables cannot be negative. The optimal result will be:

$$g^* = g(a^*, b^*) = \min_{a,b}\{g(a, b)\},$$

where $*$ means the optimal value for both function and variables. Note that different objective functions can be defined. In what follows, we will discuss the optimization based on two objective functions: minimum average T and Min–Max T [28].

4.1. Minimum Average T Objective

In this case, we want to minimize the average T over the area $A = \{(\theta_s, \theta_p) \mid \theta_s \in [0, 2\pi)$ and $\theta_p \in (0, \pi/9]\}$. Note that the case for $\theta_p = 0$ is excluded because it will

Table 2.
Optimization results for minimum average objective

Case	Measure	Initial value (a, b)	Start value g_{ave}	Final value (a^*, b^*)	Stop value g^*_{ave}	Steps
1	sum	(0.05, 0.06)	70.0967	(0.0333, 0.03)	69.2773	5
2	sum	(0.06, 0.05)	70.0967	(0.0333, 0.03)	69.2773	7
3	max	(0.05, 0.06)	17.5242	(0.0333, 0.03)	17.3193	7
4	max	(0.06, 0.05)	17.3932	(0.0333, 0.03)	17.3193	6

lead to the first special case $(T_1' - T_3')\cos\theta_s + (T_2' - T_4')\sin\theta_s \neq 0$. The objective function is thus defined as:

$$g_{\text{ave}}(a, b) = \frac{1}{A}\int_A \delta(\theta_s, \theta_p, a, b)\,\mathrm{d}A.$$

It is difficult to obtain the analytical expression for $g_{\text{ave}}(a, b)$ because even the expression of T_i for each cable is rather complicated, as discussed before. However, it is possible to use the numerical integration method and the adaptive Simpson quadrature in MATLAB [34] is employed to obtain the double integral g_{ave}.

g_{ave} is a nonlinear function of a and b, which can be seen from the derivation of the analytical expression for T_1. As a result, the quasi-Newton nonlinear optimization algorithm in MATLAB Optimization Toolbox [35] is used to minimize g_{ave}. Since the algorithm does not guarantee the convergence to the global minima, we try two different initial points to obtain the final result. Moreover, we plot the 3-D graph for $g_{\text{ave}}(a, b)$ to check the optimization results.

The optimization results for the minimum average T with different measures are shown in Table 2. From Table 2, we can see that with different initial points, the optimal results are the same and the results for different measures are also the same. The 3-D graph for $g_{\text{ave}}(a, b)$ is shown in Fig. 9. From Fig. 9, we can see the optimization results are correct. Furthermore, the surface shapes for both cases are very similar. From the optimization results, we can choose $(a^*, b^*) = (0.0333, 0.03)$ for future implementation if we want the minimize average of T.

4.2. Min–Max T Objective

The min–max objective is to minimize the maximum value for T over the area A; therefore, the function is defined as:

$$g_{\max}(a, b) = \max_A \delta(\theta_s, \theta_p, a, b).$$

It is also difficult to obtain the analytical expression for $g_{\max}(a, b)$. We discretize θ_s and θ_p, and evaluate the value at the resulting points. By dense discretization, we can obtain the function value for $g_{\max}(a, b)$ [28]. The optimization results for the min–max T with the two measures are shown in Table 3. From Table 3, we can also see that, with different initial points, the optimal results using the same measure

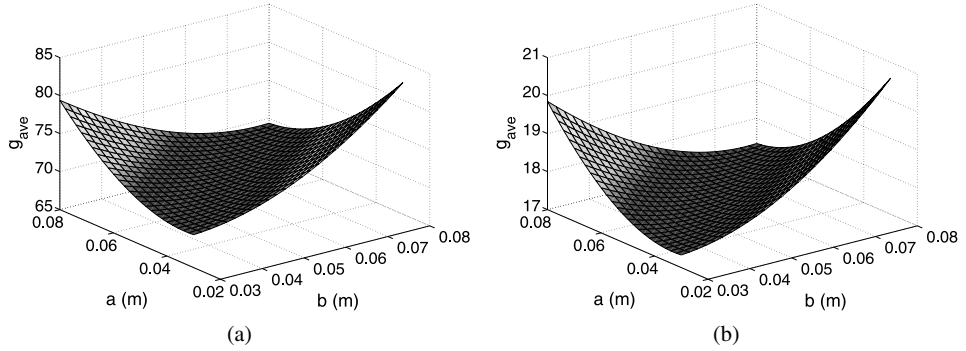

Figure 9. Average T objective function g_{ave}. (a) T_{sum}. (b) $T_{\max}$.

Table 3.
Optimization results for minimum average objective

Case	Measure	Initial value (a, b)	Start value g_{ave}	Final value (a^*, b^*)	Stop value g^*_{ave}	Steps
1	sum	(0.05, 0.06)	72.6832	(0.0392, 0.03)	70.8045	7
2	sum	(0.06, 0.05)	71.0266	(0.0392, 0.03)	70.8045	7
3	max	(0.05, 0.06)	25.6046	(0.08, 0.0747)	23.2142	9
4	max	(0.06, 0.05)	25.0912	(0.08, 0.0747)	23.2142	9

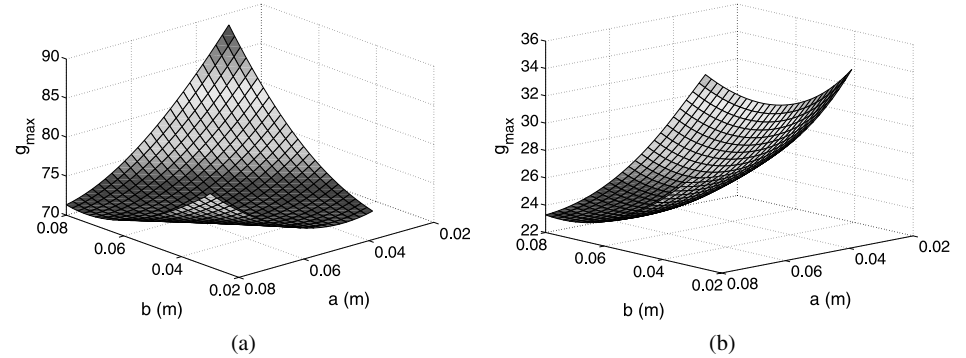

Figure 10. Maximum T objective function $g_{\max}$. (a) T_{sum}. (b) $T_{\max}$.

are the same. The results for different measures, however, are quite different with (0.0392, 0.03) for T_{sum} and (0.08, 0.0747) for $T_{\max}$.

The 3-D graphs for $g_{\max}(a, b)$ by discretizing a and b are shown in Fig. 10. From Fig. 10, we can see the above optimal points are consistent with the figures. Furthermore, although the optimal point for T_{sum} is (0.0392, 0.03), there are many non-optimal points whose function value g_{ave} is close to g^*_{ave}, which can be seen from the large area with almost the same color. In fact, for the point (0.08, 0.0747),

we have $g_{\text{ave}} = 71.0521$, which is only 0.2475 from g^*_{ave}. Therefore, we can choose $(a^*, b^*) = (0.08, 0.0747)$ for future implementation if we want to minimize the maximum value of T.

5. Conclusions

This paper gives a general solution to the inverse position and statics for a cable-driven parallel mechanism with a spring as the spine. Different from traditional parallel mechanisms, we show that the inverse position and statics should be solved simultaneously because of the parasitic motion due to the spring. The parasitic motion is obtained using the spring's lateral buckling equations. Numerical implementations verify the correctness of the proposed mathematical model. Based on the combined inverse position and statics analysis, optimal design for where to place the four cables is performed. Different optimization results are obtained if different measures are considered. It is better to place the cables close to the center if the average of cable forces should be minimized, while it is better to place the cables far from the center if the maximum cable forces should be minimized. The analysis performed in this paper can be applied to other parallel mechanisms with flexible spines.

References

1. B. Gao, N. Xi, Y. Shen, J. Zhao and R. Yang, Development of a low motion-noise humanoid neck: Statics analysis and experimental validation, in: *Proc. IEEE Int. Conf. on Robotics and Automation*, Anchorage, AK, pp. 1203–1208 (2010).
2. A. A. White and M. M. Panjabi, *Clinical Biomechanics of the Spine*, 2nd edn. JB Lippincott, Philadelphian, PA (1990).
3. A. Albers, S. Brudniok, J. Ottnad, C. Sauter and K. Sedchaicham, Upper body of a new humanoid robot — the design of ARMAR III, in: *Proc. IEEE/RAS Int. Conf. on Humanoid Robots*, Genova, pp. 308–313 (2006).
4. I. W. Park, J. Y. Kim, B. K. Cho and J. H. Oh, Control hardware integration of a biped humanoid robot with an android head, *Robotics Autonomous Syst.* **56**, 95–103 (2008).
5. J. D. Han, S. Q. Zeng, K. Y. Tham, M. Badgero and J. Y. Weng, Dav: a humanoid robot platform for autonomous mental development, in: *Proc. 2nd Int. Conf. on Development and Learning*, Cambridge, MA, pp. 73–81 (2002).
6. R. Beira, M. Lopes, M. Praca, J. Santos-Victor, A. Bernardino, G. Metta, F. Becchi and R. J. Saltaren, Design of the robot-Cub (iCub) head, in: *Proc. IEEE Int. Conf. on Robotics and Automation*, Orlando, FL, pp. 94–100 (2006).
7. T. Hashimoto, S. Hitramatsu, T. Tsuji and H. Kobayashi, Development of the face robot SAYA for rich facial expressions, in: *Proc. SICE–ICASE Int. Joint Conf.*, Busan, pp. 5423–5428 (2006).
8. F. Nori, L. Jamone, G. Metta and G. Sandini, Accurate control of a human-like tendon-driven neck, in: *Proc. IEEE Int. Conf. on Humanoid Robots*, Pittsburgh, PA, pp. 371–378 (2007).
9. I. Toshima, S. Aoki and T. Hirahara, An acoustical tele-presence robot: TeleHead II, in: *Proc. IEEE/RSJ Int. Conf. on Intelligent Robots and Systems*, Sendai, pp. 2105–2110 (2004).
10. H. Kawano, H. Ando, T. Hirahara, C. Yun and S. Ueha, Application of a MDOF ultrasonic servomotor in an auditory tele-existence robot, *IEEE Trans. Robotics* **21**, 790–800 (2005).

11. I. Mizuuchi, S. Yoshida, M. Inaba and H. Inoue, The development and control of a flexible-spine for a human-form robot, *Adv. Robotics* **17**, 179–196 (2003).
12. S. Behzadipour and A. Khajepour, Cable-based robot manipulators with translational degrees of freedom, in: *Industrial Robotics: Theory, Modeling and Control*, S. Cubero (Ed.), pp. 211–236. InTech, Rijeka (2006).
13. J. Albus, R. Bostelman and N. Dagalakis, The NIST robotcrane, *J. Robotics Syst.* **10**, 709–724 (1993).
14. K. Maeda, S. Tadokoro and T. Takamori, On design of a redundant wire-driven parallel robot warp manipulator, in: *Proc. IEEE Int. Conf. on Robotics and Automation*, Detroit, MI, pp. 895–900 (1999).
15. B. Zi, B. Y. Duan, J. L. Du and H. Bao. Dynamic modeling and active control of a cable-suspended parallel robot, *Mechatronics* **18**, 1–12 (2008).
16. P. H. Borgstrom, N. P. Borgstrom, M. J. Stealey, B. Jordan, G. S. Sukhatme, M. A. Batalin and W. J. Kaiser, Design and implementation of NIMS3D, a 3-D cabled robot for actuated sensing applications, *IEEE Trans. Robotics* **25**, 325–339 (2009).
17. N. Iwatsuki and T. Onoe, Motion control of wire-driven flexible link mechanism keeping stiffness against load, in: *Proc. 14th Int. Conf. on Mechatronics Technology*, Osaka, pp. 395–398 (2010).
18. P. Bosscher, A. T. Riechel and I. Ebert-Uphoff, Wrench-feasible workspace generation for cable-driven robots, *IEEE Trans. Robotics* **22**, 890–902 (2006).
19. E. Stump and V. Kumar, Workspaces of cable-actuated parallel manipulators, *ASME J. Mech. Des.* **128**, 159–167 (2006).
20. X. Diao and O. Ma, Force-closure analysis of 6-DOF cable manipulators with seven or more cables, *Robotica* **27**, 209–215 (2009).
21. C. B. Pham, S. H. Yeo, G. L. Yang, M. S. Kurbanhusen and I.-M. Chen, Force-closure workspace analysis of cabledriven parallel mechanisms, *Mech. Mach. Theory* **41**, 53–69 (2006).
22. S. Fang, D. Franitza, M. Torlo, F. Bekes and M. Hiller, Motion control of a tendon-based parallel manipulator using optimal tension distribution, *IEEE/ASME Trans. Mechatron.* **9**, 561–568 (2004).
23. M. Hassan and A. Khajepour, Optimization of actuator forces in cable-based parallel manipulators using convex analysis, *IEEE Trans. Robotics* **24**, 736–740 (2008).
24. S. R. Oh and S. K. Agrawal, The feasible workspace analysis of a set point control for a cable-suspended robot with input constraints and disturbances, *IEEE Trans. Control Syst. Technol.* **14**, 735–742 (2006).
25. A. Ming and T. Higuchi, Study on multiple degree-of-freedom positioning mechanism using wires, *Int. J. JSPE* **28**, 131–138 (1994).
26. B. Gao, J. Zhao, N. Xi and J. Xu, Combined kinematic and static analysis of a cable-driven manipulator with a spring spine, in: *Proc. IEEE Int. Conf. on Robotics and Automation*, Shanghai, pp. 2725–2730 (2011).
27. F. Takemura, K. Maeda and S. Tadokoro, Attitude stability of a cable driven balloon robot, in: *Proc. IEEE/RSJ Int. Conf. on Intelligent Robots and Systems*, Beijing, pp. 3504–3509 (2006).
28. J. Carretero, R. Podhorodeski, M. Nahon and C. Gosselin, Kinematic analysis and optimization of a new three degree-of-freedom spatial parallel manipulator, *ASME J. Mech. Des.* **122**, 17–24 (2000).
29. G. Gogu, Mobility of mechanisms: a critical review, *Mech. Mach. Theory* **40**, 1068–1097 (2005).
30. S. Timoshenko, *Theory of Elastic Stability*. McGraw-Hill, New York, NY (1936).
31. A. M. Wahl, *Mechanical Springs*. McGraw-Hill, New York, NY (1963).
32. R. Frisch-Fay, *Flexible Bars*. Butterworths, Washington, DC (1962).

33. S. Timoshenko and D. H. Young, *Advanced Dynamics*. McGraw-Hill, New York, NY (1948).
34. W. Gander and W. Gautschi, Adaptive quadrature — revisited, *BIT Numer. Math.* **40**, 84–101 (2000).
35. MATLAB, *Optimization Toolbox User's Guide, Version 5.0*, MathWorks, Natick, MA (2010).

About the Authors

Bingtuan Gao received his BE degree in Electrical Engineering and Automation, ME degree in Control Theory and Control Engineering, and PhD in Power Electronics and Electrical Drive, from Harbin Institute of Technology, Harbin, P. R. China, in 2002, 2004 and 2007, respectively. From 2008 to 2010, he was a Postdoc at the Department of Electrical and Computer Engineering, Michigan State University, East Lansing, MI, USA. He is currently an Associate Professor at the School of Electrical Engineering, Southeast University, Nanjing, P. R. China. His research interests include robotics, manufacturing automation and underactuated mechanical systems.

Jing Xu received his BE degree in Mechanical Engineering from Harbin Institute of Technology, Harbin, P. R. China, in 2003, and the PhD degree in Mechanical Engineering from Tsinghua University, Beijing, P. R. China, in 2008. From 2008 to 2010, he was a Postdoc in the Department of Electrical and Computer Engineering, Michigan State University, East Lansing, MI, USA. He is currently an Assistant Professor at the Department of Precision Instruments and Mechanology, Tsinghua University, Beijing, P. R. China. His research interests include robotics, manufacturing automation and image processing.

Jianguo Zhao received his BS degree in Mechanical Engineering from Harbin Institute of Technology, in 2005, and his MS degree in Mechatronic Engineering from Shenzhen Graduate School, Harbin Institute of Technology, Harbin, P. R. China, in 2007. He is currently working towards his PhD degree at Michigan State University, East Lansing, MI, USA. His research interests include parallel manipulators, bio-inspired robot design, micro robotics and mobile sensor networks.

Ning Xi received his DS degree in Systems Science and Mathematics from Washington University, St Louis, MO, USA, in 1993. He is the John D. Ryder Professor of Electrical and Computer Engineering and Director of the Robotics and Automation Laboratory at Michigan State University. Currently, he serves as the Head and Chair Professor of the Department of Manufacturing Engineering and Engineering Management at the City University of Hong Kong. He received the Best Paper Award in the IEEE/RSJ International Conference on Intelligent Robots and Systems (IROS), in August 1995, and the Best Paper Award in the 1998 Japan–USA Symposium on Flexible Automation. He was awarded the first Early Academic Career Award by the IEEE Robotics and Automation Society, in May 1999. He also received the Best Paper Award of *IEEE Transactions on Automation Science and Engineering*, in 2007. He was awarded the SPIE Nano Engineering Award, in 2007. In addition, he is a recipient of US National Science Foundation CAREER Award. He is a Fellow of the IEEE. At present he serves as the President of the IEEE Nanotechnology Council. His research interests include robotics, manufacturing automation, micro/nano manufacturing, nano sensors and devices, and intelligent control and systems.